analytical chemistry

Article

pubs.acs.org/ac

Sensitive Analysis of Protein Adsorption to Colloidal Gold by Differential Centrifugal Sedimentation

Adam M. Davidson,[†] Mathias Brust,[†] David L. Cooper,[†] and Martin Volk*[,‡]

[†]Department of Chemistry, University of Liverpool, Crown Street, Liverpool L69 7ZD, U.K.

[‡]Surface Science Research Centre, Department of Chemistry, University of Liverpool, Abercromby Square, Liverpool L69 3BX, U.K.

Supporting Information

ABSTRACT: It is demonstrated that the adsorption of bovine serum albumin (BSA) to aqueous gold colloids can be quantified with molecular resolution by differential centrifugal sedimentation (DCS). This method separates colloidal particles of comparable density by mass. When proteins adsorb to the nanoparticles, both their mass and their effective density change, which strongly affects the sedimentation time. A straightforward analysis allows quantification of the adsorbed layer. Most importantly, unlike many other methods, DCS can be used to detect chemisorbed proteins ("hard corona") as well as physisorbed proteins ("soft corona"). The results for BSA on gold colloid nanoparticles can be modeled in terms of Langmuir-type adsorption isotherms (Hill model). The effects of surface modification with small thiol-PEG ligands on protein adsorption are also demonstrated.

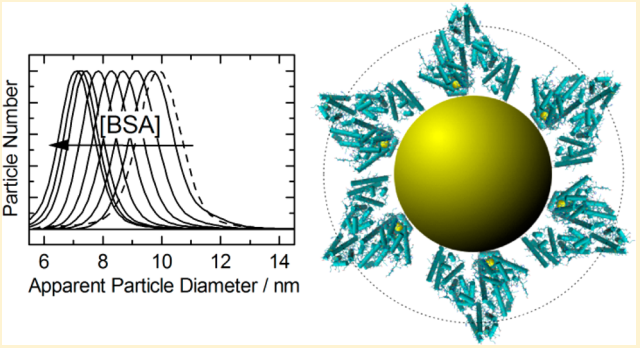

The phenomenon of protein adsorption to colloidal particles has been studied for over 100 years. Zsigmondy suggested as early as 1901 that the known protective effect of proteins on dispersions of colloidal gold was attributable to the association of proteins with the colloidal particles.[1] He also defined the *Goldzahl* (German for "gold number") as the amount of a protective agent that is able to prevent the aggregation of the gold colloid as manifested in a color change from red to blue.[1]

Both protein adsorption and the characteristic color change upon addition of some reactive agent play important roles in modern gold nanotechnology, in particular for medical diagnostics and detection.[2] These applications are behind most of the renewed interest in such adsorption phenomena. Nanoparticles (NPs) of any type, when dispersed in a biological environment, e.g., the bloodstream, will be coated by an adsorbed layer of different proteins, the so-called corona.[3−7] This can have significant consequences for the performance of the particles,[8−11] including their uptake into cells or their intended surface chemistry functionality, since important functionalities may be buried or replaced and thus inactivated by the adsorbed proteins; this may even give rise to new and potentially undesired properties. On the other hand, formation of a corona can also have beneficial effects, such as protecting functional groups, increasing blood circulation times and biocompatibility or reducing cytotoxicity.[9,11−13] With the renewed interest in protein adsorption, analytical methods that can monitor such processes and yield detailed information on the formation, structure, composition, size and stability of the corona are required. Dynamic light scattering (DLS) has been used extensively for a range of nanoscopic materials including gold to study both particle core and corona size.[14−19] A potential limitation of this method is that the particles of interest should be separated from excess protein prior to measurement to eliminate the significant contribution of unbound protein or aggregates to the signal.[7,14,15,20] DLS also has limited resolution for small monodisperse NPs.[14,21] Likewise, transmission electron microscopy (TEM) is a very powerful technique to directly image adsorbed proteins and to measure the corona thickness in preprepared samples[18] and more recently X-ray photoelectron spectroscopy has been used for this purpose,[19] but these techniques operate under UHV conditions and hence provide no information on adsorption dynamics in colloidal dispersions under equilibrium conditions. On the other hand, fluorescence correlation spectroscopy (FCS) and plasmon scattering correlation spectroscopy (PSCS) have been used to obtain diffusion coefficients and hence hydrodynamic radii of nanoparticles within protein containing fluids.[20,22−25] These can yield thermodynamic data on corona formation and have shown that the process can be quantitatively described in terms of the Hill model, i.e., Langmuir-type adsorption.

We have recently shown that differential centrifugal sedimentation (DCS) can be employed as an easy-to-use and yet highly sensitive technique to measure differences as small as the length of a single carbon−carbon bond in the ligand shell

Received: April 3, 2017
Accepted: May 17, 2017
Published: May 17, 2017

DOI: 10.1021/acs.analchem.7b01229
Anal. Chem. 2017, 89, 6807−6814

thickness of thiolate stabilized gold nanoparticles.[21] We demonstrate here that this technique is also suitable to monitor protein adsorption to gold nanoparticles and to determine the thermodynamic constants that govern this process. In addition, it is possible to distinguish between chemi- and physisorbed protein layers, sometimes called "hard" and "soft" corona, and some information on the adsorption geometry can be obtained as long as the size and shape of the adsorbate are known. DCS has been used before, chiefly to complement more extensive studies of protein corona formation on silica and polystyrene spheres[4,5,17,26] or gold nanoparticles,[19,27] but not under true equilibrium conditions, i.e., with the protein present in the centrifuge medium, which as shown below, is necessary to obtain accurate information on physisorbed layers. Unlike FCS, DCS does not require a highly sophisticated setup and does not require the addition of fluorescent labels but can be applied directly to any kind of nanoparticle; unlike PSCS, it also can be applied to small NPs which do not provide enough scattering signal for correlation spectroscopy. A related method, analytical ultracentrifugation (AUC) has recently been used for investigating protein corona formation on gold nanoparticles,[28] although no distinction was made in that report between chemi- and physisorbed coronas.

To demonstrate the usefulness of DCS for investigating chemi- and physisorbed protein layers on NPs, the adsorption of bovine serum albumin (BSA) to gold NPs with different surface functionalization was investigated. Serum albumin is one of the most abundant proteins in the blood plasma, typically present at concentrations above 10 g/L, and is the main protein in the corona formed on citrate-stabilized gold NPs in the widely used cell culture medium containing fetal bovine serum.[29] Pure BSA was used here to avoid the complexity of biological media which usually contains a mixture of proteins, sugars, and electrolytes. The gold NPs investigated were citrate-stabilized NPs, and NPs functionalized with thiolated poly(ethylene glycol) ligands having either carboxyl (PEG-COOH) or hydroxyl (PEG-OH) end groups. Citrate ligands are expected to exchange with protein, thus allowing for direct protein adsorption onto the gold NP surface; on the other hand, PEG-OH was chosen for its known lack of binding to proteins,[6,25,30] whereas PEG-COOH ligands also prevent the interaction of the protein with the gold NPs but are likely to interact directly with proteins.

EXPERIMENTAL SECTION

Chemicals. $HAuCl_4$ trihydrate; sodium citrate tribasic dihydrate, ≥99.5% purity; bovine serum albumin (BSA), ≥98%; and sucrose, ≥ 99.5%, were purchased from Sigma-Aldrich and used as supplied. Thiolated poly(ethylene glycol) ligands, $HS\text{-}(CH_2)_{11}\text{-}(EG)_6\text{-}OH$ (PEG-OH) and $HS\text{-}(CH_2)_{11}\text{-}(EG)_6\text{-}OCH_2\text{-}COOH$ (PEG-COOH), were purchased from ProChimia Surfaces and used as supplied.

Nanoparticles. Citrate-stabilized gold NPs (diameter ∼11 nm) were synthesized following a modified Turkevich-Frens method.[31,32] In brief, 20 mL of a hot 40 mM aqueous citrate solution were added to a boiling solution of 200 μmol of $HAuCl_4$ trihydrate in 200 mL of Milli-Q water and refluxed under vigorous stirring for 60 min; the solution was then cooled overnight under stirring and subsequently filtered. PEG-stabilized NPs were prepared by overnight incubation of citrate-stabilized NPs in 0.45 mM PEG, corresponding to a more than 10-fold excess with respect to the number of gold atoms on the NP surface. Excess PEG ligands were removed by at least three cycles of centrifugation (15 000 rpm, 30 min, 10 °C) and resuspension of the NPs in Milli-Q water. All samples were characterized by UV−vis spectroscopy, which showed the characteristic shift of the plasmon resonance band upon ligand exchange (Figure S1 in the Supporting Information) and by DCS (Figure 1).

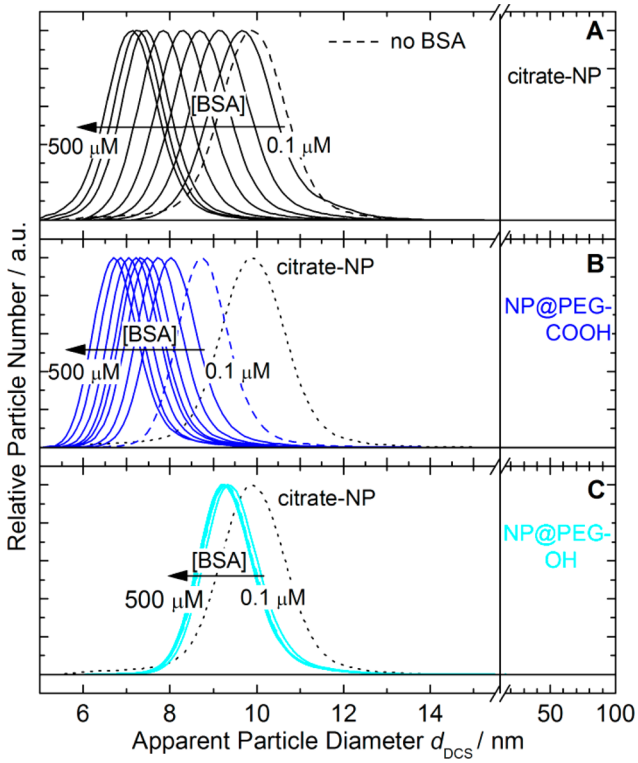

Figure 1. Size distributions for (A) citrate- and (B,C) PEG-stabilized gold NPs, before (dashed lines) and after (solid lines) 24 h incubation in BSA solutions of different concentrations, as indicated. The data shown here were obtained with the same concentration of BSA in the DCS-gradient fluid as used during NP incubation. The dotted lines in parts B and C show the distribution for citrate-stabilized NPs in the absence of BSA.

Corona Formation. BSA solutions in Milli-Q water at different concentrations were prepared freshly on the day of the experiment from stock solution (100 mg/mL). BSA solution, NP solution, and Milli-Q water were combined to yield a final NP concentration of ∼10 nM, as determined by UV−vis spectroscopy[33] and BSA concentrations in the range 0.1−500 μM. The samples were vigorously shaken and left overnight (except where stated explicitly) in standard Eppendorff tubes, which are known to be resistant to protein binding. Protein corona formation was confirmed by UV−vis spectroscopy[19,27] (Figure S1 in the Supporting Information), which for citrate-stabilized gold NPs in BSA solution showed a shift and absorbance increase of the plasmon resonance band with increasing BSA concentration, as expected for an increase of the capping layer.[33] On the other hand, only smaller changes were found for gold NPs@PEG-COOH, for which the protein corona forms at a distance of ∼3 nm from the gold core and thus has less effect on its optical properties, and no shift at all was observed for gold NPs@PEG-OH, which do not form a significant protein corona (*vide infra*). The pH, measured with a Whatman PHA230 pH meter with a Hanna Instruments microelectrode (HI 1083), of citrate-stabilized NP solutions

DOI: 10.1021/acs.analchem.7b01229
Anal. Chem. 2017, 89, 6807−6814

increased from 6.1 (no BSA) to 7.1 (high BSA concentration); the latter value corresponds to the pH of the BSA stock solution. The pH of PEG-stabilized NPs in the absence or presence of BSA was around 7 for all samples. Only where stated explicitly, excess BSA was removed after overnight incubation of citrate-stabilized NPs by three cycles of centrifugation (15 000 rpm, 30 min, 5 °C) and resuspension of the NPs in 3.6 mM citrate solution (citrate-stabilized NPs) or Milli-Q water (PEG-stabilized NPs).

UV−Visible Spectroscopy. Spectra were recorded in the range 400−800 nm using a Genesys 10S UV−vis spectrophotometer (Thermo Scientific) and a 1 cm path length cuvette.

Differential Centrifugal Sedimentation. NP size distributions were recorded using a disc centrifuge (DC24000, CPS Instruments Inc.).[21] A sucrose gradient (nine solutions in the range 8%−24% sucrose w/v in Milli-Q water or BSA solution) was filled into the disc rotating at 24 000 rpm, followed by a thin layer of dodecane, and allowed to equilibrate. The instrument was calibrated using poly(vinyl chloride) standard particles (0.226 μm, Analytik Ltd.) before *each* measurement. A minimum of three concordant measurements per sample were obtained to ensure reproducibility. All samples were gently up-turned 10 times prior to injection.

RESULTS AND DISCUSSION

Differential Centrifugal Sedimentation. DCS is a comparatively simple and easy-to-use experimental technique that physically separates NPs by size before detecting them and thereby yields highly accurate size distributions. This is achieved by sedimentation in a centrifugal disk containing a liquid whose density increases toward the outer edge, which guarantees stable sedimentation governed by Stokes' law. Near the outer edge of the disk, NPs are detected using light absorbance and scattering and their size is determined from their sedimentation time (*vide infra*). It has been shown that DCS can be used to detect differences in the size of gold NP samples and/or their ligand shell with a resolution of 0.1 nm.[21]

Figure 1 shows example size distributions for citrate- and PEG-stabilized gold NPs before and after protein corona formation by incubation in BSA solution. The data shown here were measured with BSA in the DCS-gradient fluid at the same concentration as used during incubation, distributions measured without BSA in the gradient fluid are shown in Figure S2 in the Supporting Information. These distributions show that the NP samples were highly monodisperse and that the width of the size distribution was not affected by functionalization with PEG-ligands or incubation in BSA solution, except for citrate-stabilized NPs after incubation at low BSA concentration when measured in the absence of BSA in the gradient fluid (Figure S2), for which a heterogeneous size distribution was found, ranging from slightly smaller to larger diameters than the original NPs. This can be ascribed to a partial loss of the citrate capping layer due to the reduction of citrate concentration upon addition of the BSA solution, with only some NPs adsorbing a few proteins. After incubation with ≥1 μM BSA, no such broadening was observed, indicating more homogeneous corona formation.

The size distributions shown in Figure 1 show that upon functionalization with PEG and/or protein corona formation, the apparent particle size, i.e., the size reported by the instrument, decreased. This is due to a necessary oversimplification in the analysis of the raw data, as has been noted previously.[21,34] Briefly, the instrument records the sedimentation time t which a particular fraction of the sample requires for traveling from the top of the gradient liquid to the point where they are detected. For a spherical nanoparticle with diameter d, this time is given by

$$t = \frac{C}{(\rho_{\mathrm{eff}} - \rho_{\mathrm{fl}})d^2} \tag{1}$$

where ρ_{eff} is the (effective) density of the NP, ρ_{fl} is the average density of the gradient solution, and C is a constant depending on solution viscosity, centrifuge speed, and cell geometry, which is determined using a calibration sample of known diameter. For calculating the size distribution from the distribution of sedimentation times, the operator has to specify the particle density; in the absence of information on the ligand layer thickness, the value of the core material (ρ_{Au} = 19.3 g/cm^3) is used as a realistic *a priori* approximation. Since the density of the ligand shell is significantly lower, this is an overestimation of ρ_{eff} which leads to an underestimation of the particle size, eq 1; in the case of organic molecules on gold NPs this overcompensates the actual size increase due to the ligand shell, see Figure S3 in the Supporting Information.

For a quantitative correction of this effect,[4,5,21,26] one needs to account for the effective density, ρ_{eff}, which depends on the character of the ligand shell. For a gold NP with core diameter d_{Au} and a homogeneous shell (citrate, PEG, or protein) of thickness s and density ρ_{shell}, ρ_{eff} is given by

$$\rho_{\mathrm{eff}} = \frac{d_{\mathrm{Au}}{}^3\rho_{\mathrm{Au}} + ((d_{\mathrm{Au}} + 2s)^3 - d_{\mathrm{Au}}{}^3)\rho_{\mathrm{shell}}}{(d_{\mathrm{Au}} + 2s)^3} \tag{2}$$

However, for PEG-functionalized NPs, where the corona is formed on top of the layer of covalently bound ligands, one has to distinguish between the shells formed by the PEG-ligands, with thickness s_{PEG} and density ρ_{PEG}, and the protein layer, with thickness s_{Prot} and density ρ_{Prot}:

$$\rho_{\mathrm{eff}} = [d_{\mathrm{Au}}{}^3\rho_{\mathrm{Au}} + (d_{\mathrm{Au\text{-}PEG}}{}^3 - d_{\mathrm{Au}}{}^3)\rho_{\mathrm{PEG}} + ((d_{\mathrm{Au\text{-}PEG}} + 2s_{\mathrm{Prot}})^3 - d_{\mathrm{Au\text{-}PEG}}{}^3)\rho_{\mathrm{Prot}}]/(d_{\mathrm{Au\text{-}PEG}} + 2s_{\mathrm{Prot}})^3 \tag{3}$$

where $d_{\mathrm{Au\text{-}PEG}} = d_{\mathrm{Au}} + 2s_{\mathrm{PEG}}$ is the diameter of the PEG-functionalized NP before corona formation.

In line with our previous work,[21] the density of a dense capping layer (citrate, PEG) was assumed to be similar to that of proteins, i.e., 1.4 g/cm^3;[35] variation of this value by ±0.2 g/cm^3 has virtually no effect on the value of d_{Au} determined from the DCS results (*vide infra*), and only minimally affects the results for the capping layer thickness (±0.2 nm). For the effective density of the protein corona, ρ_{Prot}, on the other hand, a lower value of 1.15 g/cm^3 was assumed, to account for the fact that due to the irregular shape of proteins the corona does not constitute a closely packed layer but contains a significant amount of solvent. This value is slightly smaller than the density of hydrated protein crystals (~1.25 g/cm^3),[36] in agreement with the higher porosity expected for a thin protein corona on a NP. Similar values have been suggested previously or determined indirectly for protein coronas on NPs;[4,5,17,26,27] the value is also in full agreement with the reported water content of a BSA corona on gold NPs of 70%.[19] The uncertainty of this value is the main contribution to the uncertainty of the corona thickness s_{Prot}; the error bars shown in Figure 2 indicate the variation of s_{Prot} when varying ρ_{Prot} in the range 1.1−1.2 g/cm^3. A more detailed discussion of the

DOI: 10.1021/acs.analchem.7b01229
Anal. Chem. 2017, 89, 6807−6814

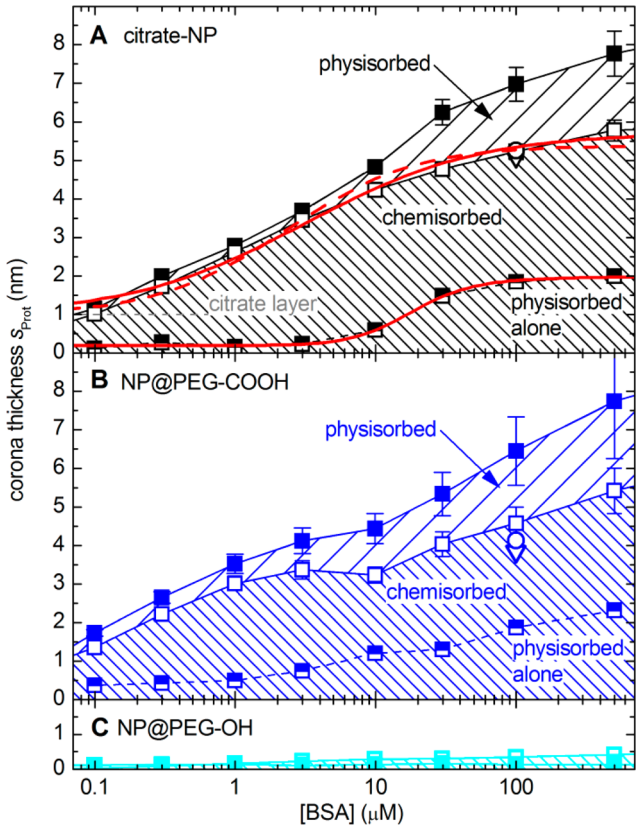

Figure 2. BSA corona thickness on (A) citrate- and (B,C) PEG-stabilized NPs after 24 h incubation at different BSA concentrations. Solid symbols refer to DCS-measurements with BSA present in the gradient fluid at the same concentration as during incubation, open symbols refer to DCS-measurements in the absence of BSA in the gradient fluid, and solid/open symbols show the difference between these results. The open circles at [BSA] = 100 μM show the results obtained immediately after removal of excess BSA from the sample by centrifugation, the open down-triangles those obtained for the same samples 24 h later. The solid red lines in panel A are fits of the data to the Hill model, eqs 5 and 6, yielding values of s_{max} = (5.7 ± 0.2) nm, K_D = (7.0 ± 2.5) μM, n = (0.75 ± 0.10) for chemisorbed BSA on citrate-NPs, and s_{max} = (2.0 ± 0.1) nm, K_D = (17.8 ± 1.5) μM, n = (2.0 ± 0.3) for the additional physisorbed protein layer; the dashed red line is a fit of the data to a Langmuir isotherm (eqs 5 and 6 for n = 1), yielding K_D = (4.1 ± 0.9) μM.

effect of this uncertainty of ρ_{Prot} is given in the Supporting Information (section S3). It should be noted that when assuming a value of ρ_{Prot} larger than 1.23 g/cm^3, no solution for eq 4 is possible for the results at the highest BSA concentrations, confirming the need to use a smaller value. In the absence of BSA in the gradient fluid, the (average) density of the gradient fluid, ρ_{fl}, is 1.064 g/cm^3. For measurements with BSA in the gradient fluid, this value was corrected for the presence of protein with higher density (1.4 g/cm^3)[35] based on the volume fraction of protein added; this correction had a measurable effect only at the highest BSA concentrations.

The instrument's analysis of the experimental sedimentation time is based on eq 1 but uses the density of gold, ρ_{Au}, in place of the correct value ρ_{eff}, so that the NP diameter reported by the instrument, d_{DCS}, relates to the correct diameter d ($d = d_{Au} + 2s$ for NPs with a single homogeneous shell consisting of citrate, PEG, or protein, $d = d_{Au} + 2s_{PEG} + 2s_{Prot}$ for PEG-functionalized NPs with protein corona) according to

$$(\rho_{eff} - \rho_{fl})d^2 = (\rho_{Au} - \rho_{fl})d_{DCS}^2 \quad (4)$$

Using the experimental result d_{DCS}, eq 4, together with either eqs 2 or 3, can be solved numerically for d_{AU} and s or $d_{Au\text{-}PEG}$ and s_{Prot}, respectively, if one of the parameters can be determined independently. In previous reports on the determination of the thickness of a chemisorbed protein corona on gold NPs, d_{Au} was determined using DLS, although it was pointed out that this may result in some inaccuracy and even account for some of the discrepancies found in these studies.[19,27] We had determined the thickness s of a citrate layer on gold NPs to be 1 nm by DCS, using a peptide (CALNN) as an "internal standard";[21] here, this value was used to determine the value of the core diameter d_{Au} from the DCS results for citrate-stabilized NPs; a value of d_{Au} = 10.8 nm was obtained for the batch of NPs used here. This value was then used for analyzing the corona thickness on citrate-stabilized NPs, where the protein is expected to replace the citrate layer, see Figure 2A, and to determine the thickness of the PEG layers, s_{PEG}, on PEG-functionalized NPs, using eq 2. Values of $s_{PEG\text{-}COOH}$ = 3.0 nm and $s_{PEG\text{-}OH}$ = 1.9 nm were obtained for the PEG-functionalized NPs in the absence of BSA. The values of d_{Au} and s_{PEG} thus determined were used to calculate the thickness of the protein corona on PEG-stabilized NPs using eq 3, see Figure 2B,C.

Corona Formation on Citrate-Stabilized NPs. Figure 2A shows a significant increase of the measured capping layer thickness after incubation of citrate-stabilized NPs with BSA for 24 h, when compared to the thickness of the citrate capping layer; this confirms that BSA forms a protein corona on gold NPs.[14−16,18,19,25,37−40] The observation that corona formation by BSA (isoelectric point, 4.7[41]) or human serum albumin (HSA), which is almost identical to BSA,[42] leads to a reduction of the negative zeta potential of citrate-stabilized gold NPs,[16,19,25] and the fact that BSA-stabilized gold NPs have the same isoelectric point as BSA[38] strongly suggest that the weakly bound citrate layer gets replaced by a protein corona which binds directly to the gold surface, although at lower BSA concentrations some citrate is expected to remain on those parts of the NP surface not covered by protein.

Most importantly, at concentrations in excess of ∼10 μM, the measured protein corona thickness depends on the presence of BSA in the gradient fluid. With BSA in the gradient fluid at the same concentration as used for incubation (solid symbols), the equilibrium between adsorbed and free protein which had been established during the 24-h incubation period is maintained throughout the measurement, so that the results reflect the thickness of the corona on nanoparticles in the presence of free protein, which may consist of tightly bound chemisorbed proteins ("hard corona") and/or loosely bound physisorbed proteins ("soft corona").

In the absence of BSA in the gradient fluid, on the other hand, a slightly thinner protein layer is found at higher BSA concentrations, indicating the loss of some of the adsorbed proteins upon injection. This loss of part of the corona within the time scale of the DCS experiment, i.e., within a few minutes, is in agreement with previous reports of such rapid removal of the physisorbed corona.[3,6] However, even the complete removal of excess BSA by repeated centrifugation prior to the DCS measurement (open circle in Figure 2A) or incubation in BSA-free citrate solution for 24 h (open triangle) do not significantly affect the measured corona thickness. This not only shows that most of the BSA adsorbed to gold NPs is

DOI: 10.1021/acs.analchem.7b01229
Anal. Chem. 2017, 89, 6807−6814

bound very strongly (chemisorbed) and is not released even upon prolonged exposure to protein-free citrate solution, but it also shows that the loss of the weakly adsorbed fraction of the corona occurs almost immediately upon injection into the gradient fluid, i.e., on a similar time scale as formation of the corona (*vide infra*). Thus, the results obtained with a BSA-free gradient fluid reflect tightly bound chemisorbed proteins ("hard corona") without the need of prior removal of excess protein from the sample.

Most of our results were obtained after incubation for 24 h to ensure full equilibration.[15] However, Figure 3 shows that most

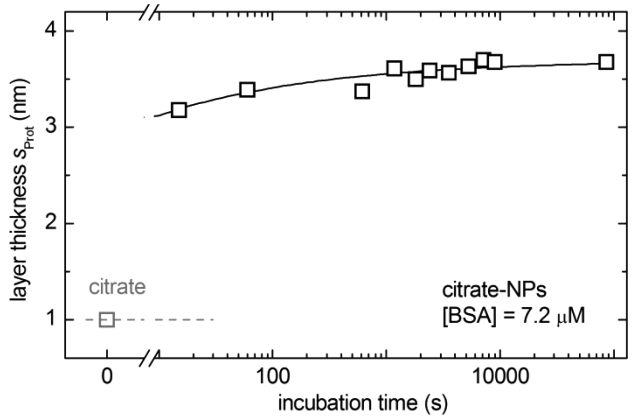

Figure 3. Variation of the BSA corona thickness formed upon incubation of citrate-stabilized NPs in 7.2 μM BSA for increasing incubation times (15 s to 24 h); the value at time zero refers to the thickness of the citrate layer; the solid line is a guide to the eye.

of the chemisorbed corona is formed on the subminute time scale: when injecting the NP/BSA mixture into a BSA-free gradient 15 s after mixing, a corona thickness corresponding to 85% of the maximum thickness is observed, with the remainder formed within 1 h. None of the previous studies attempting to observe the kinetics of formation of a chemisorbed corona had comparable time resolution, since all required extensive sample purification; therefore, it was only known that a BSA or HSA corona on citrate-stabilized NPs is formed within 15−30 min.[16,37,40] Interestingly, the process is faster than the formation of a "hard" corona, consisting largely of albumins, on citrate-stabilized gold NPs upon incubation in serum;[15] this highlights the complex kinetics of corona formation which is governed by competition between different serum components.[3,5,8,43]

Together, these results indicate that BSA rapidly forms a chemisorbed "hard" corona on citrate-stabilized gold NPs with a maximum effective thickness of 5.7 nm, in addition to which at concentrations in excess of ∼10 μM, some BSA proteins are physisorbed ("soft" corona), increasing the corona thickness by an additional 2 nm at the highest concentrations; this fraction of the corona is present only as long as the NP remains in the protein solution. It should be pointed out, however, that even at the highest BSA concentrations, BSA did not form multilayers on NPs, as had been suggested previously for BSA coronas on a variety of NPs.[22,44]

Previous reports on the formation of a chemisorbed corona of BSA or HSA on gold NPs, using DLS, yielded values of a similar order of magnitude for the corona thickness,[14−16,18,19,40] although it should be noted that DLS only poorly reproduces the size distribution of NPs in the 10−50 nm range.[14,21] DLS measurements in the presence of high concentrations of protein, on the other hand, can be distorted by contributions of unbound protein or aggregates to the signal,[14,15] and hence, to the best of our knowledge, no DLS experiments investigating the physisorbed (soft) corona have been reported for gold NPs. PCSC was used to investigate the BSA corona formed on gold NPs in the presence of high BSA concentrations, yielding values which are in agreement with the results reported here.[25] A BSA corona thickness of 3−5 nm on citrate-stabilized gold NPs was determined using TEM[18] or X-ray photoelectron spectroscopy,[19] which is in reasonable agreement with the results reported here, considering that those techniques are performed in vacuum and report on the dry ligand shell only.

Corona Formation on PEG-Functionalized NPs. Figure 2B,C summarizes the BSA corona thickness on PEG-functionalized gold NPs. NPs with a PEG-OH ligand layer form no BSA corona, not even a physisorbed "soft" corona; even with BSA present in the gradient fluid at concentrations as high as 500 μM, no significant shift of the NP size is found. This is in agreement with the general observation that PEG-OH layers lead to reduced, although not necessarily completely inhibited, protein corona formation on NPs[6,25,30] and that they prevent adsorption of BSA to gold surfaces.[45]

NPs with a carboxylated PEG (PEG-COOH) ligand layer, on the other hand, show measurable corona formation even at lower BSA concentrations, similar to that found for citrate-stabilized NPs. As for citrate-stabilized NPs, most of this corona is formed by chemisorbed proteins, since even in the absence of BSA in the gradient fluid a significant capping layer can be observed. On the other hand, it appears that chemisorptive binding of BSA to the PEG-COOH capping layer is slightly less stable than binding to citrate-stabilized gold NPs, since removal of excess BSA after formation of the corona on NP@PEG-COOH and incubation in neat water results in a slight decrease of the corona thickness (open circle and triangle at [BSA] = 100 μM in Figure 2B). For BSA concentrations exceeding 10 μM, an additional physisorbed protein layer is formed on top of the chemisorbed corona which can only be observed with BSA in the gradient fluid. It should be noted that the uncertainty of the corona thickness arising from the uncertainty of the value of ρ_{Prot} is significantly larger for these NPs than for citrate-stabilized NPs because of the increased thickness of the organic capping layer, as discussed in detail in the Supporting Information (section S3).

BSA Adsorption Isotherms. A quantitative analysis of the experimentally observed adsorption isotherms was performed using the Hill equation, which has been used previously for protein corona formation on NPs.[22,25,28] It should be noted that the Hill model assumes full equilibration on the experimental time scale and thus may not be correct for all combinations of NPs and proteins;[24,28] in fact, our observation that the removal of the chemisorbed corona in BSA-free solution takes significantly longer than 24 h raises serious doubts about the validity of this model. Thus, it is used here only as a convenient model equation and it is not meant to imply any mechanistic explanation.[46] The Hill equation predicts that the number of proteins adsorbed per NP, N, is given by

$$\frac{N}{N_{max}} = \frac{[BSA]^n}{[BSA]^n + K_D{}^n} \quad (5)$$

Here, N_{max} is the maximum number of proteins that can be adsorbed per NP, [BSA] the molar concentration of BSA, K_D

DOI: 10.1021/acs.analchem.7b01229
Anal. Chem. 2017, 89, 6807−6814

the Hill dissociation constant, i.e., the protein concentration at which half of the adsorption sites are occupied, and n the Hill coefficient which characterizes the cooperativity of adsorption. For fitting the dependence of the corona thickness on the protein concentration (Figure 2), it is assumed that the NP-protein complex adopts a spherical shape with a volume $V_{NP} + N \times V_{BSA}$, where V_{NP} denotes the volume of the nanoparticle (including the strongly bound PEG capping layer, where appropriate) and V_{BSA} the effective volume of a single protein. Thus, the effective particle diameter d is given by

$$d = d_{NP}\sqrt[3]{1 + cN} \quad (6)$$

where $c = V_{BSA}/V_{NP}$ and d_{NP} is the diameter of the NP around which the corona is formed, i.e., $d_{NP} = d_{Au}$ for citrate-stabilized NPs and $d_{NP} = d_{Au} + 2s_{PEG}$ for PEG-functionalized NPs.[47] Fits of the experimental adsorption isotherms (Figure 2) to this equation were performed with K_D, n, and $c \times N_{max}$ as free parameters using a nonlinear least-squares fitting routine (Microcal Origin); the value of $c \times N_{max}$ can then be used to calculate the maximum effective corona thickness.[48]

This model results in a good fit of the data for the chemisorbed corona on citrate-stabilized NPs, Figure 2A, yielding a maximum effective corona thickness of 5.7 nm, a Hill dissociation constant of 7 μM, and a Hill coefficient of 0.75, which indicates anticooperative behavior, presumably reflecting steric hindrance of adsorption by proteins which are already bound to the NP. In comparison, a fit to a Langmuir isotherm, which does not account for anticooperativity, yields poorer agreement with the data, see dashed line in Figure 2A; thus, the high precision of our data allows us to distinguish the effects of even weak anticooperativity. The Langmuir dissociation constant of 4.1 μM is of similar magnitude as the Langmuir dissociation constants of 0.6−2 μM reported for BSA binding to flat gold surfaces,[38] or citrate-stabilized gold NPs of 3−60 nm diameter,[14,39] although in those reports the BSA solution appears not to have been removed, suggesting that the total corona (physi- and chemisorbed) was studied.

As discussed above, the data obtained for citrate-stabilized NPs in the presence of BSA in the gradient fluid are related to the formation of a weakly bound physisorbed corona on top of the chemisorbed corona at BSA concentrations above ~10 μM. Given the complexity of this situation with two very different binding mechanisms, we do not think that fits of these data to the Langmuir or the Hill model are appropriate, although they are shown in the Supporting Information (Figure S4) for comparison with results in the literature. An estimate of the effective thickness of the physisorbed layer was obtained by subtracting the data obtained in the absence of BSA in the gradient fluid from those obtained in the presence of BSA, see Figure 2. These data were fitted to the Hill model, eqs 5 and 6, using a (BSA-concentration dependent) value for the NP diameter d_{NP} in eq 6, which includes the chemisorbed corona thickness obtained from the fit described above. This model results in a good fit, see Figure 2A, with a physisorbed corona thickness of 2.0 nm, a Hill dissociation constant K_D of 17.8 μM, which obviously is significantly larger than that of the chemisorbed corona, and a Hill coefficient of 2, indicating cooperative binding.

The adsorption isotherms of NPs with a PEG-COOH ligand layer, Figure 2B, on the other hand, are less well-defined, both for the chemisorbed corona, measured with no BSA in the gradient fluid, and the combined physi- and chemisorbed corona, measured with BSA in the gradient fluid. These isotherms suggest highly anticooperative adsorption with a Hill coefficient well below n = 0.5, although the limited concentration range prevents determination of the exact value, compare Figure S5 in the Supporting Information. For the same reason, it is not possible to provide exact values for the dissociation constant or the maximum shell thickness.

Structure of BSA Corona. Figure 4A shows the X-ray structure of BSA.[42] The protein has the shape of an equilateral triangular prism with a height of ~6.5 nm and a thickness of ~3 nm; phosphorescence depolarization results show that this shape is maintained in solution, albeit with slightly larger dimensions due to the protein hydration layer.[49] Notably, cysteine 34, which is the only cysteine not forming an intraprotein disulfide bond, is located close to the protein surface at the base of the prism and has been implicated in the formation of interprotein disulfide bonds during protein isolation.[42]

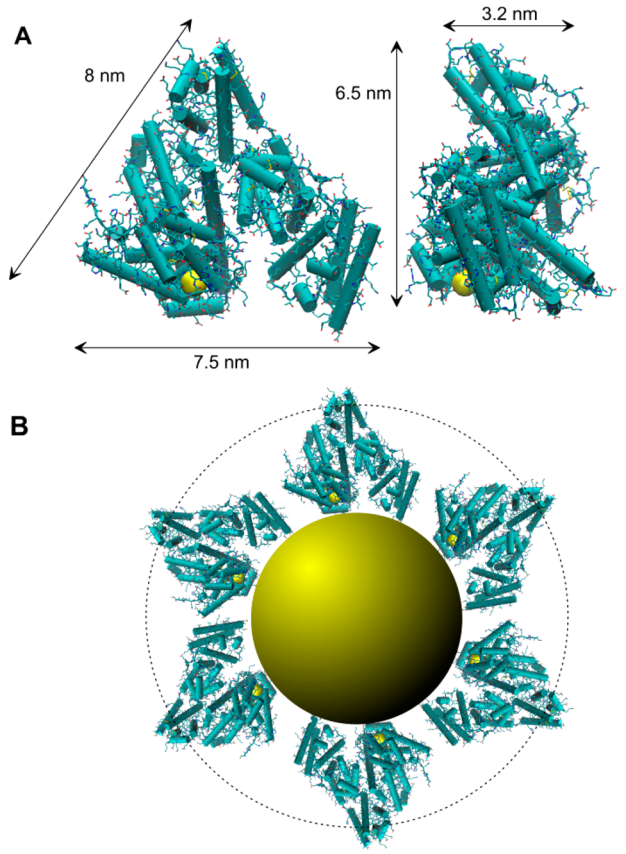

Figure 4. (A) Structure of BSA (PDB-ID 4F5S);[42] the cylinders represent α-helices, and the yellow sphere indicates the sulfur of cysteine 34 (created using VMD[52]). (B) Cartoon representation of the hard corona formed by BSA on a gold NP with 10.8 nm diameter; the dotted line indicates the effective corona thickness of 5.7 nm determined here (all size dimensions to scale).

Previously, the adsorption of HSA on FePt and CdSe@ZnS nanocrystals coated with carboxylic acid functionalized polymers (diameter 10−15 nm) had been investigated by FCS, indicating a maximum corona thickness of 3.3 nm in the presence of HSA ("soft" corona).[22] This was taken as an indication that serum albumin binds with its flat triangular surface on the NP surface, which is consistent with the existence of a patch of positive charges on one of these

DOI: 10.1021/acs.analchem.7b01229
Anal. Chem. 2017, 89, 6807−6814

triangular surfaces, suggesting electrostatic binding of serum albumin to the negatively charged NP surface.[23]

In contrast, our results show that incubation of citrate-stabilized gold NPs with BSA leads to the formation of a chemisorbed protein corona with an effective thickness of 5.7 nm. We suggest that this strong binding is achieved by the formation of a covalent bond between gold and the sulfur of cysteine 34, located at the base of the triangular prism. This leads to the formation of a layer of proteins which stand "upright" on the NP surface, as shown schematically in Figure 4B. The actual height of the protein is approximately 6.5 nm, which is compatible with the measured effective corona thickness of 5.7 nm. It should be noted that the effective hydrodynamic size (Stokes diameter) of irregularly shaped NPs with a highly corrugated surface layer, such as shown in Figure 4B, is not the same as that of a spherical NP with the same volume, even if this approximation is widely made, since the hydrodynamic drag of the "protrusions" is not completely compensated by the "depressions". Moreover, an analysis of the effective layer thickness of a protein corona also needs to account for the protein's hydration layer, which has a thickness of 0.3−1 nm.[50,51] Both of these effects are difficult to quantify; therefore, no attempt was made to quantify the number of BSA proteins adsorbed on each NP from the data.

This model of the chemisorbed BSA corona on gold NPs assumes that no significant structural changes of the protein take place when BSA binds. Gold NPs with a BSA corona are recognized by BSA-antibodies,[15] which indicates that the protein structure remains intact in the corona; this conclusion was further supported by temperature-dependent UV−vis spectroscopy results, which suggest that BSA on gold NPs is not denatured at room temperature,[53] and CD spectra of BSA bound to gold nanorods, which show that only minor structural changes occur upon binding.[54]

The suggestion that BSA is bound to gold NPs by a covalent bond contradicts the suggestion which if often found in the literature that the protein corona is formed by noncovalent interactions. However, the observation that BSA remains bound to gold NPs for at least a day (and potentially much longer) even in the absence of free BSA strongly supports this suggestion. Covalent binding between BSA and the NP also makes it likely that the protein would not easily exchange with other "hard corona" proteins in solution and may be the reason for the memory effect that has been described in the literature, i.e., the fact that the corona composition after incubation in complex biological samples depends on details of the incubation history.[11,55] In this context, it is also interesting to note that the chemisorbed BSA corona on citrate-stabilized gold NPs is formed within seconds of incubation in BSA solution, which is much faster than the usual hour time scales for hard corona formation in serum.[3,8,15] This is due to the competition between serum components with different binding modalities, including proteins with weaker but faster adsorption which rapidly cover the NP surface during the initial phase of corona formation, thus preventing fast formation of the hard corona which eventually develops.

CONCLUSIONS

It has been demonstrated that DCS can follow with high precision the subtle changes in NP size due to the formation of a protein corona upon incubation of gold NPs in protein solution, even for NPs as small as 10 nm and, most importantly, can easily provide data for both, the "soft" and the "hard" corona, i.e., the corona before and after removal of excess protein. This ability to investigate the "soft" corona is in contrast to many other techniques, in particular DLS, which require removal of excess protein or involve dilution and hence alter the corona. Since most medical applications of NPs proceed in the presence of excess protein, investigation of the "soft" corona often is more relevant than that of the "hard" corona alone. Some other techniques in principle allow the investigation of both "soft" and "hard" coronas, in particular fluorescence or scattering correlation spectroscopy[20,22−25] or analytical ultracentrifugation;[28] in comparison to these methods, DCS is an easy-to-use technique which does not require a sophisticated setup, mathematical deconvolution of the raw data, or specialist expertise. Moreover, FCS requires the presence of a fluorescent label, and PSCS suffers from comparatively poor resolution and is limited to larger NPs; none of these drawbacks affect DCS or AUC. Finally, it was shown that the kinetics of corona formation on the subminute time scale is also accessible by DCS.

ASSOCIATED CONTENT

Supporting Information

The Supporting Information is available free of charge on the ACS Publications website at DOI: 10.1021/acs.analchem.7b01229.

UV−vis spectra of NPs; DCS size distributions measured without BSA in the gradient fluid; discussion of the uncertainty of the exact value of the corona density on the results; fits of adsorption isotherms not shown in the main text (PDF)

AUTHOR INFORMATION

Corresponding Author

*Phone: ++44-151-794-3317. Fax: ++44-151-794-3588. E-mail: m.volk@liverpool.ac.uk.

ORCID

Martin Volk: 0000-0003-3555-8584

Author Contributions

The manuscript was written through contributions of all authors. All authors have given approval to the final version of the manuscript.

Notes

The authors declare no competing financial interest.

All raw data are openly available from the University of Liverpool Research Data Catalogue at http://datacat.liverpool.ac.uk/id/eprint/242.

ACKNOWLEDGMENTS

The research leading to these results has received funding from the European Research Council under the European Union's Seventh Framework Programme (Grant FP7/2007-2013)/ERC-Advanced Grant Project 321172 PANDORA. Funding by the Engineering and Physical Sciences Research Council (DTP Studentship A.M.D.) is gratefully acknowledged.

REFERENCES

(1) Zsigmondy, R. *Kolloidchemie*, 2nd ed.; Verlag von Otto Spamer: Leipzig, Germany, 1918.

(2) Wilson, R. *Chem. Soc. Rev.* **2008**, *37*, 2028−2045.

(3) Cedervall, T.; Lynch, I.; Lindman, S.; Berggard, T.; Thulin, E.; Nilsson, H.; Dawson, K. A.; Linse, S. *Proc. Natl. Acad. Sci. U. S. A.* **2007**, *104*, 2050−2055.

DOI: 10.1021/acs.analchem.7b01229
Anal. Chem. 2017, 89, 6807−6814

(4) Walczyk, D.; Bombelli, F. B.; Monopoli, M. P.; Lynch, I.; Dawson, K. A. *J. Am. Chem. Soc.* **2010**, *132*, 5761−5768.
(5) Monopoli, M. P.; Walczyk, D.; Campbell, A.; Elia, G.; Lynch, I.; Bombelli, F. B.; Dawson, K. A. *J. Am. Chem. Soc.* **2011**, *133*, 2525−2534.
(6) Walkey, C. D.; Chan, W. C. W. *Chem. Soc. Rev.* **2012**, *41*, 2780−2799.
(7) Treuel, L.; Eslahian, K. A.; Docter, D.; Lang, T.; Zellner, R.; Nienhaus, K.; Nienhaus, G. U.; Stauber, R. H.; Maskos, M. *Phys. Chem. Chem. Phys.* **2014**, *16*, 15053−15067.
(8) Maiorano, G.; Sabella, S.; Sorce, B.; Brunetti, V.; Malvindi, M. A.; Cingolani, R.; Pompa, P. P. *ACS Nano* **2010**, *4*, 7481−7491.
(9) Mahon, E.; Salvati, A.; Bombelli, F. B.; Lynch, I.; Dawson, K. A. *J. Controlled Release* **2012**, *161*, 164−174.
(10) Salvati, A.; Pitek, A. S.; Monopoli, M. P.; Prapainop, K.; Bombelli, F. B.; Hristov, D. R.; Kelly, P. M.; Aberg, C.; Mahon, E.; Dawson, K. A. *Nat. Nanotechnol.* **2013**, *8*, 137−143.
(11) Hamad-Schifferli, K. *Nanomedicine* **2015**, *10*, 1663−1674.
(12) Mahmoudi, M.; Monopoli, M. P.; Rezaei, M.; Lynch, I.; Bertoli, F.; McManus, J. J.; Dawson, K. A. *ChemBioChem* **2013**, *14*, 568−572.
(13) Wang, F.; Yu, L.; Monopoli, M. P.; Sandin, P.; Mahon, E.; Salvati, A.; Dawson, K. A. *Nanomedicine* **2013**, *9*, 1159−1168.
(14) Tsai, D.-H.; DelRio, F. W.; Keene, A. M.; Tyner, K. M.; MacCuspie, R. I.; Cho, T. J.; Zachariah, M. R.; Hackley, V. A. *Langmuir* **2011**, *27*, 2464−2477.
(15) Casals, E.; Pfaller, T.; Duschl, A.; Oostingh, G. J.; Puntes, V. *ACS Nano* **2010**, *4*, 3623−3632.
(16) Goy-Lopez, S.; Juarez, J.; Alatorre-Meda, M.; Casals, E.; Puntes, V. F.; Taboada, P.; Mosquera, V. *Langmuir* **2012**, *28*, 9113−9126.
(17) Minelli, C.; Garcia-Diez, R.; Sikora, A. E.; Gollwitzer, C.; Krumrey, M.; Shard, A. G. *Surf. Interface Anal.* **2014**, *46*, 663−667.
(18) Cui, M.; Liu, R.; Deng, Z.; Ge, G.; Liu, Y.; Xie, L. *Nano Res.* **2014**, *7*, 345−352.
(19) Belsey, N. A.; Shard, A. G.; Minelli, C. *Biointerphases* **2015**, *10*, 019012.
(20) Huehn, D.; Kantner, K.; Geidel, C.; Brandholt, S.; De Cock, I.; Soenen, S. J. H.; Gil, P. R.; Montenegro, J.-M.; Braeckmans, K.; Muellen, K.; Nienhaus, G. U.; Klapper, M.; Parak, W. J. *ACS Nano* **2013**, *7*, 3253−3263.
(21) Krpetić, Ž.; Davidson, A. M.; Volk, M.; Lévy, R.; Brust, M.; Cooper, D. L. *ACS Nano* **2013**, *7*, 8881−8890.
(22) Röcker, C.; Poetzl, M.; Zhang, F.; Parak, W. J.; Nienhaus, G. U. *Nat. Nanotechnol.* **2009**, *4*, 577−580.
(23) Maffre, P.; Nienhaus, K.; Amin, F.; Parak, W. J.; Nienhaus, G. U. *Beilstein J. Nanotechnol.* **2011**, *2*, 374−383.
(24) Milani, S.; Bombelli, F. B.; Pitek, A. S.; Dawson, K. A.; Raedler, J. *ACS Nano* **2012**, *6*, 2532−2541.
(25) Dominguez-Medina, S.; McDonough, S.; Swanglap, P.; Landes, C. F.; Link, S. *Langmuir* **2012**, *28*, 9131−9139.
(26) Kelly, P. M.; Åberg, C.; Polo, E.; O'Connell, A.; Cookman, J.; Fallon, J.; Krpetic, Ž.; Dawson, K. A. *Nat. Nanotechnol.* **2015**, *10*, 472−479.
(27) Bell, N. C.; Minelli, C.; Shard, A. G. *Anal. Methods* **2013**, *5*, 4591−4601.
(28) Bekdemir, A.; Stellacci, F. *Nat. Commun.* **2016**, *7*, 13121.
(29) Fleischer, C. C.; Kumar, U.; Payne, C. K. *Biomater. Sci.* **2013**, *1*, 975−982.
(30) Hong, R.; Fischer, N. O.; Verma, A.; Goodman, C. M.; Emrick, T.; Rotello, V. M. *J. Am. Chem. Soc.* **2004**, *126*, 739−743.
(31) Turkevich, J.; Stevenson, P. C.; Hillier, J. *Discuss. Faraday Soc.* **1951**, *11*, 55−75.
(32) Frens, G. *Nature (London), Phys. Sci.* **1973**, *241*, 20−22.
(33) Haiss, W.; Thanh, N. T. K.; Aveyard, J.; Fernig, D. G. *Anal. Chem.* **2007**, *79*, 4215−4221.
(34) Jamison, J. A.; Krueger, K. M.; Yavuz, C. T.; Mayo, J. T.; LeCrone, D.; Redden, J. J.; Colvin, V. L. *ACS Nano* **2008**, *2*, 311−319.
(35) Fischer, H.; Polikarpov, I.; Craievich, A. F. *Protein Sci.* **2004**, *13*, 2825−2828.
(36) White, E. T.; Tan, W. H.; Ang, J. M.; Tait, S.; Litster, J. D. *Powder Technol.* **2007**, *179*, 55−58.
(37) de Roe, C.; Courtoy, P. J.; Baudhuin, P. *J. Histochem. Cytochem.* **1987**, *35*, 1191−1198.
(38) Brewer, S. H.; Glomm, W. R.; Johnson, M. C.; Knag, M. K.; Franzen, S. *Langmuir* **2005**, *21*, 9303−9307.
(39) Chakraborty, S.; Joshi, P.; Shanker, V.; Ansari, Z. A.; Singh, S. P.; Chakrabarti, P. *Langmuir* **2011**, *27*, 7722−7731.
(40) Khan, S.; Gupta, A.; Verma, N. C.; Nandi, C. K. *J. Chem. Phys.* **2015**, *143*, 164709.
(41) Peters, T. *Adv. Protein Chem.* **1985**, *37*, 161−245.
(42) Bujacz, A. *Acta Crystallogr., Sect. D: Biol. Crystallogr.* **2012**, *68*, 1278−1289.
(43) Fleischer, C. C.; Payne, C. K. *Acc. Chem. Res.* **2014**, *47*, 2651−2659.
(44) Yu, S.; Peralvarez-Marin, A.; Minelli, C.; Faraudo, J.; Roig, A.; Laromaine, A. *Nanoscale* **2016**, *8*, 14393−14405.
(45) Silin, V.; Weetall, H.; Vanderah, D. J. *J. Colloid Interface Sci.* **1997**, *185*, 94−103.
(46) Goutelle, S.; Maurin, M.; Rougier, F.; Barbaut, X.; Bourguignon, L.; Ducher, M.; Maire, P. *Fundam. Clin. Pharmacol.* **2008**, *22*, 633−648.
(47) For citrate-stabilized NPs, an offset of 1 nm was added to *d*, eq 6, to account for the citrate layer present in the absence of BSA, which gets progressively replaced upon increasing [BSA].
(48) V_{BSA} is the corona volume associated with one protein, including a significant amount of water, compare Figure 4, and is not known, so that it is not possible to determine N_{max} from $c \times N_{max}$.
(49) Ferrer, M. L.; Duchowicz, R.; Carrasco, B.; de la Torre, J. G.; Acuna, A. U. *Biophys. J.* **2001**, *80*, 2422−2430.
(50) Merzel, F.; Smith, J. C. *Proc. Natl. Acad. Sci. U. S. A.* **2002**, *99*, 5378−5383.
(51) Shiraga, K.; Ogawa, Y.; Kondo, N. *Biophys. J.* **2016**, *111*, 2629−2641.
(52) Humphrey, W.; Dalke, A.; Schulten, K. *J. Mol. Graphics* **1996**, *14*, 33−38.
(53) Teichroeb, J. H.; Forrest, J. A.; Ngai, V.; Jones, L. W. *Eur. Phys. J. E: Soft Matter Biol. Phys.* **2006**, *21*, 19−24.
(54) Wang, L.; Li, J.; Pan, J.; Jiang, X.; Ji, Y.; Li, Y.; Qu, Y.; Zhao, Y.; Wu, X.; Chen, C. *J. Am. Chem. Soc.* **2013**, *135*, 17359−17368.
(55) Lundqvist, M.; Stigler, J.; Cedervall, T.; Berggard, T.; Flanagan, M. B.; Lynch, I.; Elia, G.; Dawson, K. *ACS Nano* **2011**, *5*, 7503−7509.

DOI: 10.1021/acs.analchem.7b01229
Anal. Chem. 2017, 89, 6807−6814